MedCrave
Step into the World of Research
Material Science & Engineering International Journal

Review Article

Open Access
CrossMark

Structural changes of TiO_2 as a result of CNTs incorporation

Abstract

The subject of this research work was to analyze the structural and morphological changes of TiO_2 as a result of incorporation of CNTs and interpret the underlying principles for the observed interactions. Hybrid TiO_2/CNTs nanostructures were prepared by simplified sol-gel method followed by monitoring the thermally-induced alterations occurring up to 400 ºC. The effects of different type of CNTs (activated MWCNTs and as prepared SWCNTs) as well as the variation of the content of MWCNTs in association with the metal-dopant (Pt or Co) influencing the structural parameters of TiO_2 was monitored. Addition of CNTs and metallic phase causes reduction of TiO_2 (anatase) crystallite size. The applied instrumental techniques such as XRPD, Raman spectroscopy and thermal (TG, DTA and DTG) analysis points out on achieved interaction between TiO_2 and incorporated CNTs. Morphological changes, observed from the SEM micrographs, revealed better inter-locking of the TiO_2 matrix with SWCNTs than with MWCNTs. Formation of a more structurally disordered and non-stoichiometric anatase phase seemed to be a preferred choice for the obtained TiO_2-CNT-metalic phase nanocomposites for further utilization in sensor-design products.

Keywords: TiO_2/CNTs nanocomposites, sol-gel, structural changes, morphology.

Volume 6 Issue 2 - 2022

Perica Paunović, Anita Grozdanov, Petre Makreski, Iva Dimitrievska, Aleksandar Petrovski

[1]Faculty of Technology and Metallurgy, SS Cyril and Methodius University, Macedonia
[2]Institute of Chemistry, Faculty of Natural Sciences and Mathematics, SS Cyril and Methodius University, Macedonia

Correspondence: Anita Grozdanov. Faculty of Technology and Metallurgy, SS Cyril and Methodius University, R. N. Macedonia, Email anita.grozdanov@yahoo.com

Received: May 20, 2022 | **Published:** May 27, 2022

Introduction

Relatively low price, high chemical stability and appropriate physical properties with an emphasis of the semi conductivity, make the nanostructure TiO_2 applicable in a wide range of technical and technological purposes. The suitable properties of TiO_2 are affected by the existence of three natural crystalline forms: rutile, anatase and brookite. The first two polymorphs are the most abounded and pile up the most of the applications, whereas brookite found less common interest due to the complex synthesis procedure. The crystalline lattice of rutile and anatase is the tetragonal, differing in the lattice parameters and their spatial orientation (a = 3.733 Å, c = 9.370 Å for anatase and a = 4.584 Å, c = 2.953 Å for rutile).[1] The elementary building unit of TiO_2 is consisted of one titanium atom coordinated by 6 oxygen atoms in a TiO_6 octahedral fashion.[2] The connection of these octahedral by vertices favors formation of anatase crystalline structure while connection by edges builds up the rutile structure. In brookite, the octahedral are connected by both edges and vertices forming an orthorhombic structure (a = 5.436 Å, b = 9.166 Å, c = 5.135 Å).[2-4]

The most important and crucial property of TiO_2 for the variety of applications lies in its semi conductivity of n-type with $3d^2 4s^2$ outer electron distribution.[5] This electronic structure of semiconducting TiO_2 is appropriate for photo catalysis and sensing application. The valence band (O-2p states) is non-receptive to holes whereas the conduction band (Ti-3d states) is receptive to electrons promoting the conductivity only from the electrons in the undoped TiO_2.[6] Thus, TiO_2 is considered as semiconductor with wide band (3 eV for rutile and 3.2 eV for anatase).[7] The conductivity is very low at ambient temperature and slightly increases at elevated temperatures. Due to mentioned crystalline and electronic structure, TiO_2 demonstrates great potential as photo catalyst and gas sensor.

The main and the most widespread fields of applications are connected with environmental monitoring and protection (Figure 1), such as: *i*) photo catalytic remediation including water purification,[8] photo catalytic degradation of toxic, hardly degradable cyclic organic compounds in air and aqueous media,[9] dye degradation in textile industry[10] etc.; *ii*) alternative, environmental friendly energy sources such as photo catalytic water splitting,[11] dye sensitized solar cells,[12] electrode material in Li ions batteries,[13] electrode material in hydrogen electrolyses/fuel cells,[14] component of support material for electro catalysts,[15] *iii*) sensors for detecting of variety of gases (H_2, NO_2, NO_x, CO, CO_2, O_2, NH_3, H_2S, CF_6) and VOCs (methanol, ethanol, propanol, and acetone)[5,6,16,17] and anti-bacterial activity in health protection.[18] Fujishima and Honda[19] pioneered water splitting using TiO_2 (rutile) semiconductor photo electrode and Pt counter electrode that marked a new era in heterogeneous catalysis followed by enormous number of researches concerned with photo catalytic processes in the field of energy production and environmental protection using TiO_2 as photo catalyst. Among the different TiO_2 structural forms, anatase has been recognized as the most active photo catalyst, although exhibits higher band gap energy.[7] TiO_2 based gas sensors are typical resistant-type sensors demonstrating a decrease or increase of resistance when probing the monitored gas, with sensing two-step process mechanism: receptor process and transducer process. The receptor process occurs at the TiO_2 surface, including physisorption and chemisorptions processes, while the transducer process includes the transportation of electrons in the TiO_2 and the transformation of electrons into the outward resistance signal.[17]

There are several approaches for improvement the performances of TiO_2 (shift photo catalytic activity to the visible light region, increasing the conductivity etc.) such as: *i*) doping with anions (N, C, F or B) or cations (Fe, Co, Ni or Cr), affecting lattice defects, mainly oxygen vacancies,[20] *ii*) transformation to non-stoichiometric titanium oxides (Magneli phases) filled with lattice defects of oxygen vacancies type[21] and *iii*) irradiation of TiO_2 by some ionizing radiation(electron beam, X-rays, or γ-rays).[22]

Carbon nanotubes (CNTs) with their superior mechanical, electrical, thermal and surface properties showcase immense potential for incorporation in the nanostructured TiO_2 materials that improve their performance as a result of the following reasons:

i) Within the variety of electronic properties, CNTs have large electron-storage capacity. Therefore, the photon-excited electrons from valence to conductive band of TiO_2 are kept, and consequently prolong the recombination of the electron-hole pairs, providing good chemical interaction with adsorbed pollutant species, i.e. their faster and complete degradation;[23]

ii) Considering the semi conductive properties of CNTs (very low energy of band gap), the synergetic interaction with TiO_2 leads to increasing the photo catalytic activity of TiO_2 in the region of the visible light. Therefore, CNTs act as a photosensitizer in the TiO_2/CNTs composite photo catalysts;[24]

iii) As result of the high specific surface area (400–900 m^2/g^{-1}forSWCNTs and 200–400 $m^2/g^{-1}$for MWCNTs),[25] CNTs improve the adsorption capacity and dispersion of TiO_2 within the TiO_2/CNTs nanocomposites. The hollow morphology and high surface area of CNTs deliver more active centers and surface groups available either for photo catalytic reaction or for sensing the gases.[23,26]

The preparation of TiO_2/CNTs nanocomposites is based on the different methods aimed for TiO_2 synthesis[27] such as: mechanical mixing with or without sonication, hydrothermal, solvothermal, sol-gel techniques, deposition techniques of liquids (LPD), aerosol (AD), chemical vapor (CVD), spin coating, electro spinning etc.

The aim of this work is focused to elucidate the observed structural changes that occurred within the fabricated TiO_2/CNTs nanocomposites. The products were prepared by sol-gel method, while testing different approaches that comprise variation of the CNTs amount, selection of both SWCNTs and MWCNTs and nanocomposites doping with two metals (Pt and Co).

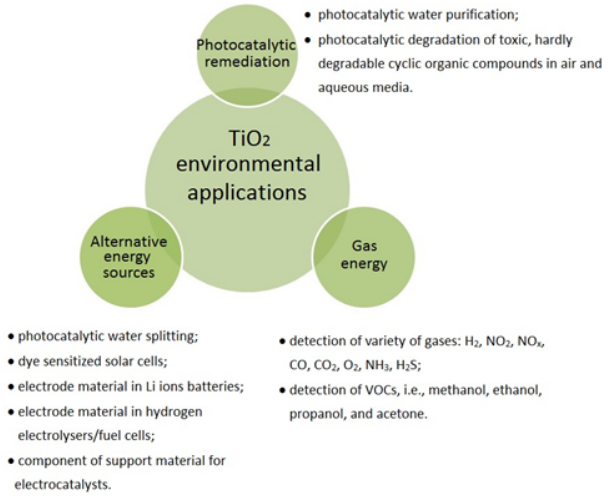

Figure 1 The main fields of TiO_2 application.

Materials and methods

The studied TiO_2/CNTs nanocomposites were prepared by sol-gel method and subsequent thermal treatment (calcination) in chamber furnace (Figure 2). In the first step of the process, carbon nanotubes (activated MWCNTs-COOH and SWCNT, provided by Cheap Nano, China) were dispersed in non-polar organic solvent – anhydrous ethanol (Merck, PA). Dispersion was performed on a magnetic stirrer at 900 rpm for 30 minutes at ambient temperature. In the second step, titanium tetraisopropoxide (TTIP) (Aldrich, 97%) was added into the dispersion in ethanol: TTIP high ratio of 8:1 due to the TTIP sensitivity to moisture. To avoid slow reaction of TTIP with the moisture from the air, an immediate hydrolysis was carried out. For such purpose, 1M HNO_3 was used in the ratio TTIP: HNO3 = 10:1. For fabrication of the metal-doped samples, first HNO_3 was added, followed by supplementation of Me-accac (Me-2,4-pentanedionate, Me = Co or Pt, Alfa Aesar) dissolved in ethanol. Evaporation of the solvent was carried out at atmospheric pressure, temperature of 48 ºC and velocity of stirring of 600-900 rpm, until a nanoscaled black powder of $Ti(OH)_4$/CNTs was obtained. The thermal treatment of the $Ti(OH)_4$/CNTs powder was carried out in a chamber furnace in an air atmosphere for 2h, at 400 °C to set the temperature region of anatase stability. The composition of the studied composite sample is shown in the Table 1. In order to observe the structural changes within the composite samples, pure TiO_2 was prepared by the same procedure and pure CNTs were characterized.

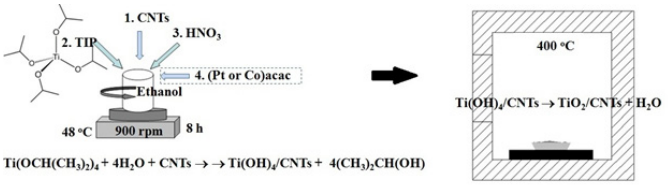

Figure 2 Schematic view of sol-gel procedure for synthesis of the studied TiO_2/CNTs.

Table 1 Numeration and composition (%, wt.) of the studied material's samples

Sample	Composition
TiO2	100%TiO2
1	80%TiO2 + 20% MWCNTs-COOH
2	70%TiO2 + 30% MWCNTs-COOH
3	78.4%TiO2 + 19.6% MWCNTs-COOH + 2% Pt
4	78.4%TiO2 + 19.6% MWCNTs-COOH + 2% Co
5	80%TiO2 + 20% SWCNTs
MWCNTs-COOH	100% MWCNTs-COOH
SWCNTs	100% SWCNTs

The structural analysis (identification of the present structure phases and structural parameters) was performed by Scanning Electron Microscopy (SEM), X-ray powder diffraction (XRPD)and Raman spectroscopy. SEM observation of the prepared samples was performed by using a Scanning Electron Microscope –JEOL JSM-IT200. Rigaku Ultima IV diffract meter with Cu*K*α radiation (λ = 1.54178 Å) was employed for XRPD measurements. An X-ray tube voltage was set to 40 kV and the current to40 mA using the *K*β filter. The diffraction patterns were recorded in 20 to 80 º range (2θ) at a rate of 5 º/min on a D/teXUltra high-speed (1D) detector. Interplanar distances and lattice parameters were determined and the average crystallite size was calculated from the XRPD peaks using the Scherrer's equation.[28] Horiba Jobin Yvon Lab Ram 300 Infinity was used for collection of the micro-Raman spectra. ANd: YAGfrequency doubled laser operating at 532 nm was selected without attenuation filter. An Olympus MPlanN confocal microscope with ×50 long-distance objective for was chosen, whereas the pinhole aperture and the entrance slit were set to 100 and 500 microns, respectively. Raman peak of silica wafer positioned at 520.7 cm^{-1}assisted in calibration of the Raman shift. A grating of 1800 grooves/mm was selected to disperse the signal onto the CCD detector providing high dispersion and a high spectral resolution. All bands were fitted using a mixed Gaussian-Lorentz function, and a solution converged to minimum after a maximum of 50 iterations. Linear function was used for baseline corrections.

Citation: Paunović P, Grozdanov A, Makreski P, et al. Structural changes of TiO_2 as a result of CNTs incorporation. *Material Sci & Eng.* 2022;6(2):31–39. DOI: 10.15406/mseij.2022.06.00177

Thermal stability of the studied samples was tested using Perkin Elmer PYRIS Diamond Thermo gravimetric/Differential Thermal Analyzer (TGA/DTA/DTG). According to the standard procedure guided in an air flow atmosphere, about 20 mg of the samples were heated in the range of 25–850 ºC applying the heating rate of 40 ºC·min^{-1}.

Results and discussion

The surface morphology of pure TiO_2 (Figure 3a) depicted aggregates with irregular geometric shape separated by the presence of cracks and holes. As a result of the cracks existence, the material possesses trans-particle porosity while the holes contribute to the inter-particle porosity. This observation favors the catalytic ability, but also serve as stabilizer to better embed and inter-lock the of carbon nanotubes when creation of TiO_2/CNTs nanocomposites takes place. It is apparent that the functionalized MWCNTs-COOH blocks are split during their acid activation to sustain diameters of 20 to 40 nm (Figure 3b). The morphology of nanocomposites with composition 80%TiO_2 + 20% MWCNTs-COOH (Sample 1) illustrated shortened carbon nanotubes that are loosely embedded and weakly locked into the TiO_2 matrix (Figure 3c). Similar morphology was observed in the composite sample additionally doped by 2 wt.% of metallic phase (samples 3 and 4, Figure 3e and Figure 3f). The microscopy analysis inferred that metallic nanoparticles are well dispersed among both the TiO_2 grains and carbon nanotube, without noticeable agglomeration. The stability was explained by the surface functional groups on the functionalized MWCNTs, such as the carboxylic (–COOH) and carbonyl (–C=O) groups, which may foster and improve the dispersion of metal nanoparticles, providing further interactions between the metallic nanoparticles, TiO_2 and carbon nanotubes that was confirmed by other analytical techniques (XRD and Raman).

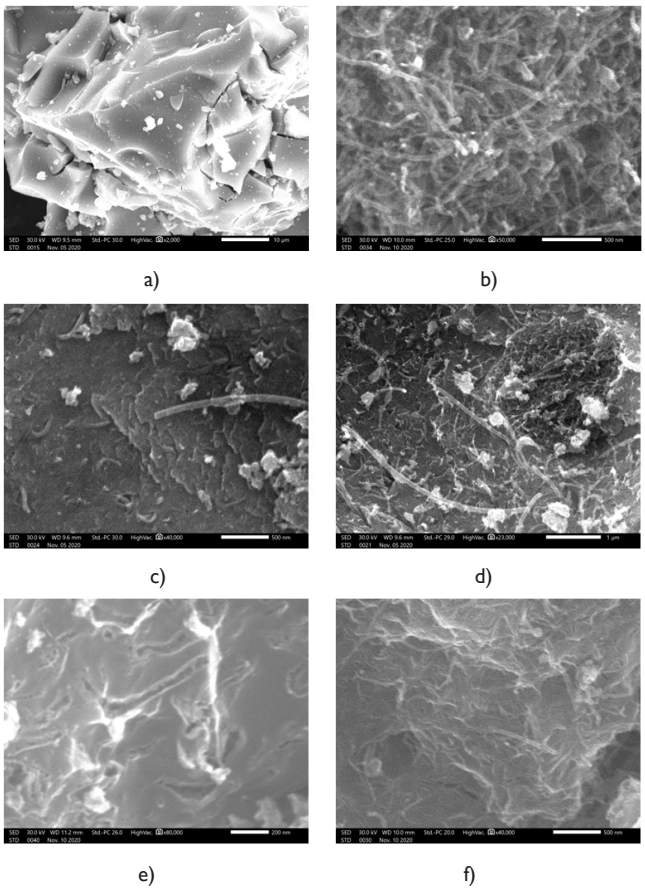

a) b) c) d) e) f)

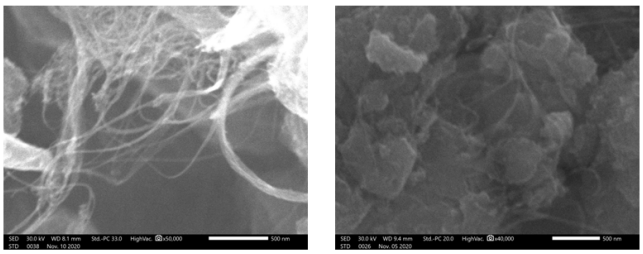

g) h)

Figure 3 SEM images of the studied samples: a) TiO_2, b) MWCNTs-COOH, c) nanocomposite 80%TiO_2 + 20% MWCNTs-COOH, d) nanocomposite 70%TiO_2 + 30% MWCNTs-COOH, e) nanocomposite 78.4%TiO_2 + 19.6% MWCNTs-COOH + 2% Pt, f) nanocomposite 78.4%TiO_2 + 19.6% MWCNTs-COOH + 2% Co, g) SWCNTs and h) nanocomposite 80%TiO_2 + 20% SWCNTs.

Much improved embedding and inter-locking of the MWCNTs-COOH within the TiO_2 matrix was observed for nanocomposites with 30% MWCNTs-COOH (sample 2, Figure 3d). Here, interaction between TiO_2 and MWCNTs-COOH is expressed by covering the TiO_2 surface with the carbon nanotubes, indicating that the homogeneity of the coating MWCNTs layer formed on TiO_2 will be obtained by adjusting the MWCNT to TiO_2 weight ratio. The representation of the morphology of the SWCNTs (Figure 3g) outlined particles with smaller diameter than MWCNTs (2-5nm) and considerable length in micrometers attributed to the lack of additional chemical treatment. In contrary to the nanocomposites with 20 % wt. MWCNTs, where the embedding and inter-locking in the TiO_2matrix was poor, here, the equal quantity of SWCNTs (sample 5) provided favorable entrenchment of the SWCNTs within the TiO_2 matrix (Figure 3h).

X-ray powder diffraction (XRPD) diagrams of different TiO_2/CNTs composites and pure TiO_2 (Table 1) depicted more or less prominent peaks (Figure 4a). The determined 2θ angles (attributed to the corresponding indices) positioned at ~25.3º (101), ~36.9º (103), ~37.8º (004), ~38.6º (112), ~48.1º (200), ~53.9º (105), ~55.1º (211), ~68.7º (116), ~70.3º (220), ~75.1º (215) pointed out on formation of anatase crystalline modification at 400 ºC.[29,30] Moreover, the XRPD patterns showcase revealed more pronounced, sharper, and intensive diffraction peaks in the pure TiO_2 in comparison to the composite samples. An addition of CNTs decreased peak intensity and induced broadening of the anatase peaks attributed to the lowered size of the TiO_2 crystallites. Furthermore, the positions of the composites' peaks were lowered for 0.03-0.06º 2θ values in comparison to the corresponding peaks found in pure TiO_2.

The characteristic XRPD peaks for pure graphitic carbon phase (Figure 4b, top) were positioned at ~25.9º (002), ~43.0º (100), ~44.1º (101), ~53.4º(004) and ~78.3º (110) that nicely agrees with the literature data.[31,33] The latter two maxima were not evidenced in the pattern of the SWCNTs (Figure 4b, bottom). However, all peaks resulting from the carbon phases almost disappeared in the diagrams of the studied composites except for the most intensive one (~25.9 º, 002) (Figure 4a). Due to the lower crystalline extent of MWCNTs than that of TiO_2, this peak was shielded and overlapped by the strongest (101) anatase peak at ~25.3 º (Figure 4a, bottom). [34]

In the XRPD pattern of the composite containing 2 wt% platinum (Figure 4a, sample 3), characteristic peak emerged at 39.75º which corresponds to (111) crystal planes in face-centered cubic (fcc) Pt[35,36]. Due to the insignificant platinum content, the peak was barely evidenced in the summarized diagrams plot (Figure 3a) and separately

Citation: Paunović P, Grozdanov A, Makreski P, et al. Structural changes of TiO_2 as a result of CNTs incorporation. *Material Sci & Eng.* 2022;6(2):31–39.
DOI: 10.15406/mseij.2022.06.00177

presented for clarity (Figure 4c). The other characteristic Pt maxima at 46.24º (200) and 67.44º (220) were not observed, which indicated that Pt atoms were distributed and majorly incorporated into the TiO_2 matrix.[36] On contrary, the diagram of the composite containing 2 wt.% cobalt (sample 4) showed no characteristic peaks from its presence (Figure 4a) probably due to the very small particle size (several nm). Such size is assumed taking into considerations our similar composites (72% MWCNTs, 18% TiO_2 and 10% Co) where 2 nm cobalt particles were determined when composite fabrication was guided by the corresponding organometallic precursor and the same sol-gel method.[37-39]

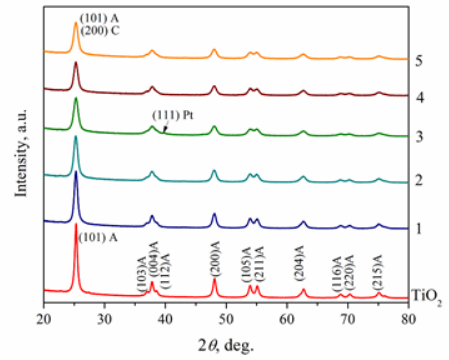

a)

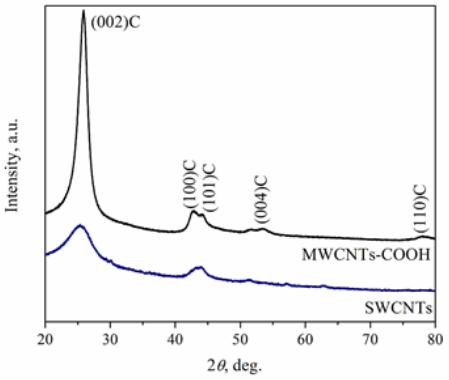

b)

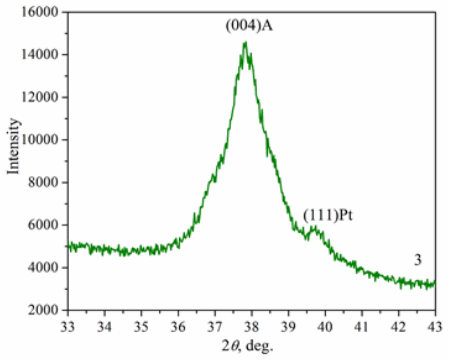

c)

Figure 4 XRPD spectra of a) TiO_2/CNTs nanocomposites and pure TiO_2, b) pure MWCNTs-COOH and SWCNTs and c) magnified part of the XRPD spectrum of sample 3 (TiO_2/MWCNTs/Pt) where characteristic peak of Pt appears.

The structural changes within the dominant crystalline TiO_2phase of the studied composites were estimated by the values of some crystalline parameters such as Interplanar distance ($d_{\{h,k,l\}}$), lattice parameters (*a* and *c*, for the tetragonalanatase system) and crystallite size (D) using the following equations:

$$2 \cdot d_{(hkl)} \cdot \sin\theta = n \cdot \lambda \,, \tag{1}$$

$$\frac{1}{d_{(hkl)}} = \frac{h^2 + k^2}{a^2} + \frac{l^2}{c^2} \,, \tag{2}$$

$$D = \frac{K \cdot \lambda}{FWHM \cdot \cos\theta} \,, \tag{3}$$

where, *K* - constant (0.94), λ- X-ray wavelength (1.54178 Å), FWHM - full width at half maximum of the peak considered for calculation (101 and 200), θ- angle of the diffraction peak, *n*- positive integer, (*hkl*) - Miller indices of the corresponding crystal plane, *a* and *c*- lattice parameters of tetragonal crystal lattice of TiO_2.

The results of these calculations are summarized in the Table 2. In general, interplanar distance and lattice parameters of the TiO_2/CNTs composites increased that demonstrated expansion of the crystal lattice as a result of the TiO_2 and CNTs interaction. The doped metallic phase (Pt or Co) also takes part in the interaction with the TiO_2 and CNTs when samples 3 and 4 are considered.

The values of crystallite size (Table 2) also inferred that involving the carbon nanotubes in the TiO_2 phase reduced the size of the TiO_2 crystallites. With addition of 20 wt.% MWWCNTs-COOH in the nanodimensional TiO_2 (sample 1), the size of the crystallites shrunk from ~17 to ~13 nm (Table 2). Further increase of the MWWCNTs-COOH amount to 30 wt.% (sample 2) strongly reduced the crystallite size (~11 nm). Doping 2 wt.% metallic phase in the composite system 1 (samples 3 and 4) resulted in further decline of size to ~9.5 and 10.5 nm, respectively. By comparing the effect of addition of different types of carbon nanotubes (samples 1 and 5), it was found that inclusion of the SWCNTs significantly promoted the reduction of TiO_2 particles (reduction from ~17 to ~10 nm) compared to the MWCNT (reduction from ~17 to ~13 nm) (Table 2).

The Raman spectra of the studied materials are shown in three panels, separately showing different wave number regions (Figure 5). The bands from the TiO_2 vibration modes (Figure 5a) evolved in the first 100-800 cm^{-1}region, whereas the bands assigned to the vibrational modes of MWCNTs (Figure 5b) and SWCNTs emerged (Figure 5c) in the 1100-1800 cm^{-1} region.

The uniform Raman spectra results (Figure 5a) confirmed the sole existence of the anatase crystalline phase in all studied samples. The results confirmed anatase stability upon doping with metals and CNTs showing no occurrence of solid-solid transformation to other known TiO_2 polymorphs (brookite and rutile). Namely, Raman spectra correspond to the well-known spectrum of anatase single crystal identified by Oshaka et al.[40] consisted of the following bands attributed to the Raman vibration modes: E_g positioned at 144, 197, and 639 cm^{-1}, B_{1g}positioned at 399 cm^{-1}, and the A_{1g} and B_{1g}doublet positioned at 514 cm^{-1}. Analogous to XRPD pattern, the Raman spectrum of the pure TiO_2 exhibited most pronounced bands compared to the other samples. Following the addition of the CNTs in the studied materials, the spectral bands reduced their intensity and somewhat lost the sharp shape. The band broadening and loss of the intensity was attributed to the smaller particles of the composite materials[34,41] as well as to the induced defects such as oxygen vacancies[42-44] causing non-stoichiometry in the anatase structure. It was also evident that the positions of the corresponding Raman bands were shifted to lower

Citation: Paunović P, Grozdanov A, Makreski P, et al. Structural changes of TiO_2 as a result of CNTs incorporation. *Material Sci & Eng.* 2022;6(2):31–39. DOI: 10.15406/mseij.2022.06.00177

wavenumbers (red shift) for the composite spectra compared to pure TiO_2. The positions of the Raman vibrational modes characteristic for TiO_2 are summarized in Table 3. Considering the reduction of the crystallite size as a result of the involving of the CNTs in the composite materials and taking into consideration the phonon confinement model, it was expected that the vibrational modes, especially for the most prominent E_g mode, should be shifted to higher wave numbers (blue shift).[22,41,45] Nonetheless, this expectation seems applicable for the pure TiO_2 system whereas, for the composites of TiO_2 with carbon nanotubes, the red shift can be attributed to the strong interaction between TiO_2 and CNTs, i.e. due to bonding between TiO_2 layer and CNTs core (formation of Ti-O-C bonds) causing distortion of the TiO_2 structure.[46,47] On the other hand, if the frequency of phonons interacting with the incident photon decreases, and consequently, the studied material is under tensile strain (expansion of the crystalline lattice), the red shift (decrease) of the wavenumber of the Raman vibrational modes should be expected. The latter result nicely complements to the XRPD observations.

The Raman spectra of MWCNTs-COOH and composites containing MWCNTs-COOH are shown in Figure 5b, where structural changes of CNTs can be observed after mixing with TiO_2more pronounced with addition of the multiwalled carbon nanotubes. D band (1350 cm^{-1}) is the second-order Raman vibrational mode, characteristic for disordered carbon indicating mostly structural defects such as vacancies and edges in the tubes, and other carbonaceous impurities.[48] G band (1580 cm^{-1}) is the only first order Raman vibrational mode,[48] indicating highly oriented graphitic structure. This band is associated with intercalated graphite compounds (but not graphite), increasing disorder by functionalization and strain in the C–C bond vibrations.[49] D, G and D' bands for pure MWCNTs-COOH, are positioned at 1333.46, 1570.76 and 1604.03 cm^{-1}, respectively (Table 4). In the spectra of the corresponding composite materials, all bands are shifted to higher wavenumbers. The upshift served as an indicator for a strong interaction between TiO_2 and MWCNTs-COOH, enhancing the charge transfer from TiO_2 to MWCNTs-COOH in order to separate and stabilize the charge and thereby hinder charge recombination.[34,50] Similar behavior of the D and G bands was observed in the systems including SWCNTs (Figure 5c) where the blue shift is less pronounced compared to the systems involving the MWCNTs-COOH phase.

Table 2 Changes of interplanar distance, lattice parameters, and crystallite size of the studied samples

Sample	2q (°)	FWHM	d-value (Å)	a (Å)	c (Å)	Crystallite size (nm)	Average crystallite size (nm)
TiO2	25.31	0.494	3.5175	3.7832	9.5546	17.22	16.87
	48.08	0.551	1.8916			16.52	
1	25.29	0.643	3.5216	3.7872	9.5724	13.23	12.815
	48.05	0.733	1.8936			12.4	
2	25.27	0.762	3.5249	3.789	9.6098	11.17	11.005
	48.02	0.838	1.8945			10.84	
3	25.29	0.864	3.5212	3.7874	9.5612	9.85	9.62
	48.04	0.968	1.8937			9.39	
4	25.28	0.784	3.5225	3.7888	9.5647	10.86	10.555
	48.02	0.886	1.8944			10.25	
5	25.28	0.839	3.5233	3.7888	9.5807	10.14	10.005
	48.02	0.921	1.8944			9.87	

Table 3 Band positions of the Raman vibrational modes characteristic for anatase (in cm^{-1})

Sample	Eg	Eg	B1g	A1g +B1g	Eg
TiO2	140.42	194.23	394.35	515.29	638.55
1	137.1	187.74	388.05	508.71	631.05
2	138.63	188.47	389.07	508.43	630.51
3	136.07	186.2	386.79	507.1	630.81
4	135.24	186.61	386.14	506.4	629.51
5	133.13	184.5	384.99	505.1	628.06

Table 4 Band positions of the Raman vibrational modes characteristic for CNTs (in cm^{-1})

Sample	D	G	D'	ID/IG	ID/IG	ID/IG
1	1343.55	1577.61	1613.01	1.2	1.51	1.71
2	1342.5	1578.09	1613.54	1.11	0.92	1.1
3	1341.9	1573.97	1610.13	0.97	1.42	1.26
4	1344.43	1576.81	1615.587	0.91	1.51	1.34
5	1335.35	1577.84	/	0.05	0.58	0.03
MWCNTs-COOH	1333.46	1570.76	1604.03	1.35	1.06	1.51
SWCNTs	1331.55	1576.78	/	0.03	0.88	0.02

Thermal properties of TiO_2/CNTs nanocomposites were tested by TGA/DTA/DTG measurements (Figure 6-8, Table 5). The first thermal degradation temperatures (T_{dI}), depending on the fabricated sample, spans from 130 to 180°C, and the corresponding mass loss is attributed to the evaporation of solvents and water. Under the air flow, the MWCNTs-COOH sample remained stable at somewhat higher temperature (595.6 °C) compared to the SWCNT (489.7 °C). These temperatures are in accordance to the reported oxidation temperature of CNTs samples (550–750 °C), which limits the calcination (or heat treatment) temperature to improve the crystallization during TiO_2/CNTs nanocomposites synthesis.[51,52] Taking into account this temperature interval, the treatment of TiO_2/CNTs nanocomposite samples favors rutile formation and CNTs oxidation.[53,54]

Citation: Paunović P, Grozdanov A, Makreski P, et al. Structural changes of TiO_2 as a result of CNTs incorporation. *Material Sci & Eng.* 2022;6(2):31–39. DOI: 10.15406/mseij.2022.06.00177

Furthermore, it was observed that the critical temperature in terms of mass loss due to the oxidation of nanotubes extents from590 to 660 °C (Figure 6) that is readily observed from the derivative thermogravimetry data (DTG2, Table 5). The constant levels observed after 600°C in TGA curves should correspond to the complete oxidation of nanotubes.

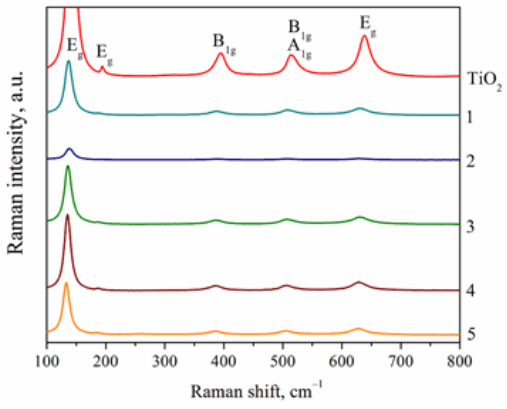

a)

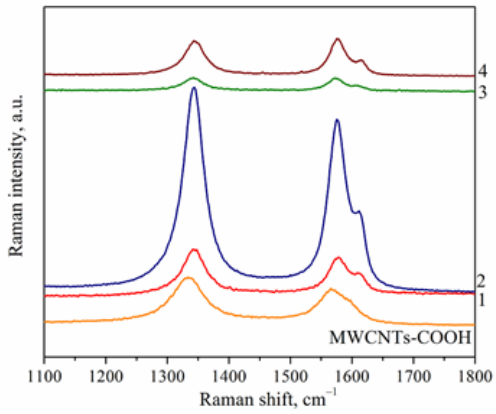

b)

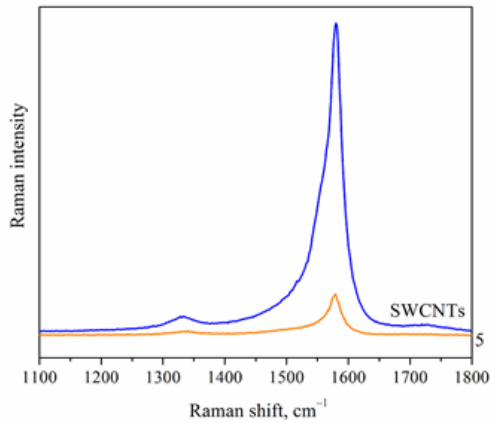

c)

Figure 5 Raman spectra of a) TiO_2/CNTs nanocomposites and pure TiO_2 in the region of 100 to 800 cm^{-1}, b) pure MWCNTs-COOH and nanocomposites containing MWCNTs-COOH (samples 1–4) in the region of 1100 to 1180 $cm^{-1}$and c) pure SWCNTs and nanocomposite containing SWCNTs (sample 5) in the region of 1100 to 1180 cm^{-1}.

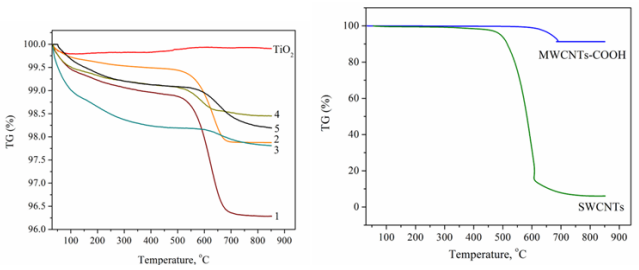

a) b)

Figure 6 TGA curves (weight loss) of a) TiO_2/CNTs nanocomposites and pure TiO_2 and b) pure MWCNTs-COOH and SWCNTs.

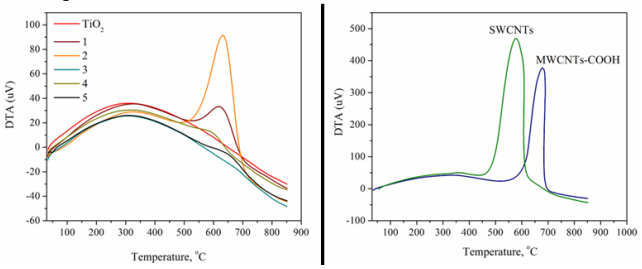

a) b)

Figure 7 DTA curves of a) TiO_2/CNTs nanocomposites and pure TiO_2 and b) pure MWCNTs-COOH and SWCNTs.

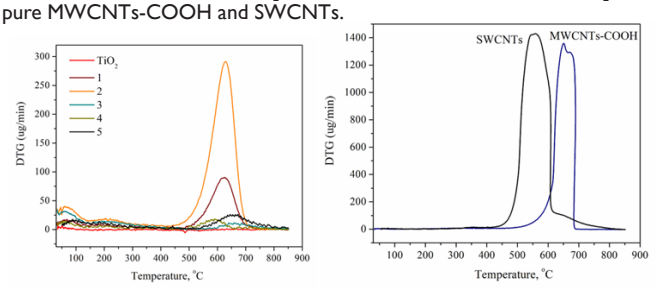

a) b)

Figure 8 DTG curves of a) TiO_2/CNTs nanocomposites and pure TiO_2 and b) pure MWCNTs-COOH and SWCNTs.

Incorporation of CNTs into the TiO_2 phase structure decreased the thermal stability of the pure TiO_2that remained thermally stable up to 676 °C. Namely, adding 30% (wt.) of MWCNTs-COOH in the nanocomposite content decreased the thermal stability up to 120 °C which is also lower than the T_{d2} of the neat MWCNTs-COOH (563.7 vs. 676.2 °C). The similar effect was registered for both types of CNTs, MWCNTs-COOH and SWCNTs (Table 5). On contrary, the TiO_2/SWCNT nanocomposite (sample 5) showed higherT_{d2}value compared to the corresponding T_{d2} of pure SWCNTs (594.3 vs. 489.7 °C). Such observation might postulate that the mixing of SWCNTs with TiO_2stabilized the nanocomposite and indicate even distribution and dispersion of SWCNTs in the TiO_2 phase. Comparing the effect of further incorporation of two metallic phases (Pt- and Co-doping) in the TiO_2/MWCNT nanocomposites, it was found that Co-doped sample decreased the thermal stability of the corresponding composite (T_{d2} = 535.4 °C vs. T_{d2} = 604.4 °C, Table 5).

Lower thermal degradation temperatures for the studied TiO_2/CNTs nanocomposites indicate that the crystalline structure of TiO_2 was disordered that harmonizes to the XRPD analysis. Reduction of TiO_2 crystallites sizes resulted in lower thermal stability of TiO_2/CNTs nanocomposites, which is agreement with the theory that crystallites with lower dimension exhibit lower thermal stability.[51]

Citation: Paunović P, Grozdanov A, Makreski P, et al. Structural changes of TiO_2 as a result of CNTs incorporation. *Material Sci & Eng.* 2022;6(2):31–39. DOI: 10.15406/mseij.2022.06.00177

Table 5 Characteristic TGA oxidation temperatures and DTG and DTA transformation points (in °C)

Sample	TiO2	1	2	3	4	5	MWCNT-COOH	SWCNT
Td1	/	134.4	147.5	166.1	154.8	180.5	/	/
Td2	676.2	563.7	548.3	604.4	535.4	594.3	595.6	489.7
Td3	809.4	/	/	/	679.3	/	/	/
DTG 1	/	66.6	222.4	208	208.7	181	651.6	559.8
DTG 2	/	626.1	630.8	658.7	592.1	663.9	/	/
DTG 3	/	/	/	/	716.7	/	/	/
DTA1	322	328.1	328	315.3	318.6	313.4	333	575max
DTA2	/	621.2	634.6	/	587.1	636.7	677.3max	/

Conclusion

The presented research was motivated by the idea to produce and characterize nanocomposites based on TiO_2 and CNTs, which can be used for different application, e.g. gas sensors or photocatalysts. Different samples were selected and the influence of different types of CNTs, their content and addition of metallic phase was evaluated. According to the obtained results, the following conclusions were drawn:

1. TiO_2 predominantly influences on the morphology of the studied nanocomposites, resulting in the presence of cracks and holes between the aggregates. Due to the presence of cracks, the material possesses trans-particle porosity, while the holes contribute to inter-particle porosity. Improved inter-locking of the TiO_2 matrix was obtained by SWCNTs in comparison to MWCNTs because the activation treatment of MWCNTs shortened the nanotubes. However, as the content of MWCNTs increases, the inter-locking of the TiO_2 matrix has been improved.
2. XRD analysis determined the anatase crystalline form of TiO_2. The addition of the CNTs reduced TiO_2 crystallite size and further increase of the MWCNTs content delivered larger reduction of the TiO_2 crystallite size. Also, the addition of the metallic phase contributes to reduction of TiO_2 crystallites. SWCNTs provided stronger reduction effect of the crystallite size. In general, interplanar distances and lattice parameters of the TiO_2/CNTs composites have shown increased values, suggesting expansion of the crystal lattice as a result of the TiO_2 and CNTs interaction. The doped metallic phase, also takes part in the interaction with the TiO_2 and CNTs phases.
3. According to the Raman analysis, the addition of the CNTs in the studied materials reduced the intensity and widened the spectral bands pointing out to the smaller particles of the composite materials than pure TiO_2. Also, the positions of the corresponding Raman bands were shifted to lower wavenumbers (red shift) for composite samples compared to those of pure TiO_2. The band downshift was attributed to the strong interaction between TiO_2 and CNTs, i.e. due to bonding between TiO_2 layer and CNTs core (formation of Ti-O-C bonds) causing distortion of the TiO_2 structure. On the other hand, decrease of the frequency of phonons interacting with the incident photon, suggests that the studied material is under tensile strain (expansion of the crystalline lattice), which is in a good agreement with increasing of the interplanar distance observed by the XRPD analysis.
4. Lower thermal degradation temperatures for the studied TiO_2/CNTs nanocomposites indicate that the crystalline structure of TiO_2 was disordered that nicely complemented to the XRPD analysis. Reduction of TiO_2 crystallites sizes resulted in lower thermal stability of TiO_2/CNTs nanocomposites that agree with the theory that crystallites with lower dimension exhibit lower thermal stability.

Formation of a more structurally disordered and non-stoichiometric anatase phase seemed to be a preferred choice for the obtained TiO_2-CNT-metalic phase nanocomposites in order to be used as sensors. Namely, it was explained, for hydrogen sensing mechanism,[26] that the hydrogen molecules are first chemisorbed and dissociated on metallic phase, and spill out of the metallic surface, diffusing into the TiO_2 surface layer, with MWCNTs providing a preferential pathway to the current flow.

Acknowledgments

This paper is part of the work realized in the project titled "Application of functional nano particles and structures in facial health masks and filters for protection of Covid 19", financed by UNESCO Participation program for R.N. Macedonia (2020-2021).

Conflicts of interest

Authors declare that there is no conflict of interest.

References

1. Diebold U. The surface science of TiO_2. *Surf Sci Rep*. 2003;48:53–229.
2. Landmann M, Rauls E, Schmidt WG. The electronic structure and optical response of rutile, anatase and brookite TiO_2. *J Phys: Condens Matter*. 2012;24(19):195503-1−195503-6.
3. Lam SM, Sin JC, Abdullah AZ, et al. Photocatalytic TiO_2/carbon nanotube nanocomposites for environmental applications: An overview and recent developments. *Fullerenes Nanotubes Carbon Nanostruct*. 2014;22:471–509.
4. Paunović P, Petrovski A, Načevski G, et al. Pathways for the production of non-stoichiometric titanium oxides. *Nanoscience Advances in CBRN Agents Detection, Information and Energy Security*. 2015;239–253.
5. Tang J, Zhang X, Xiao S, et al. Application of TiO_2 nanotubes gas sensors in online monitoring of S_{F6} insulated equipment. *Intech Open Science*. 2017.
6. Zhang J, Zhao C, Hu PA, et al. A UV light enhanced Ti_{O2}/graphene device for oxygen sensing at room temperature. *RSC Adv*. 2013;3:22185–22190.
7. Zhang J, Zhou P, Liu J, et al. New understanding of the difference of photocatalytic activity among anatase, rutile and brookite TiO_2. *Phys Chem Chem Phys*. 2014;16:20382–20386.
8. Nakata K, Fujishima A. TiO_2 photocatalysis: design and applications. *J Photochem Photobiol C*. 2012;13(3):169–189.
9. Ameta R, Benjamin S, Ameta A, et al. Photocatalytic degradation of organic pollutants: a review. *Mater Sci Forum*. 2013;34:247–272.
10. Cisneros RL, Espinoza AG, Litter MI. Photodegradation of an azo dye of the textile industry. *Chemosphere*. 2012;48:393-399.

Citation: Paunović P, Grozdanov A, Makreski P, et al. Structural changes of TiO_2 as a result of CNTs incorporation. *Material Sci & Eng*. 2022;6(2):31–39.
DOI: 10.15406/mseij.2022.06.00177

11. Ni M, Leung MKH, Leung DYC, et al. A review and recent developments in photocatalyticwater-splitting using TiO_2 for hydrogen production. *Renewable Sustainable Energy Rev*. 2007;11:401–425.

12. Ahmad MS, Pandey AK, Rahim NA. Advancements in the development of TiO_2 photoanodes and its fabrication methods for dye sensitized solar cell (DSSC) applications. A review. *Renewable Sustainable Energy Rev*. 2017;77:89–108.

13. Liu Y, Yang Y. Recent progress of TiO_2-based anodes for Li ion batteries. *J Nanomater*. 2016;2016:1–15.

14. Abdullah N, Kamarudin SK. Titanium dioxide in fuel cell technology: An overview. *J Power Sources*. 2015;278:109–118.

15. Paunović P. Enhancing the Activity of Electrode Materials in Hydrogen Economy. LAP Lambert Academic Publishing, 2018, p.22.

16. Maziarz W, Kusior A, Trenczek-Zajac A. Nanostructured TiO_2-based gas sensors with enhanced sensitivity to reducing gases. *Beilstein J Nanotechnol*. 2016;7:1718-1726.

17. Wang Y, Wu T, Zhou Y, et al. TiO_2-Based nanoheterostructures for promoting gas sensitivity performance: designs, developments, and prospects. *Sensors*. 2017;17(9):711–35.

18. Grozdanov A, Paunović P. Functionalized nanoparticles in facemasks for protection of Covid 19. *Material Sci & Eng*. 2021; 5(5):142–146.

19. Fujishima A, Honda K. Electrochemical photolysis of water at a semiconductor electrode. *Nature*. 1972;238:37–38.

20. Zaleska A. Doped-TiO_2: A Review. *Recent Pat Eng*. 2008;2:157–164.

21. Toyoda M, Yano T, Tryba B, et al. Preparation of carbon-coated Magneli phases Ti_nO_{2n-1} and their photocatalytic activity under visible light. *Appl Catal B*. 2009;88:160–164.

22. Paunović P, Grozdanov A, Makreski P, et al. Structural changes of TiO_2 as a result of irradiation by e-beam and x-rays. *J Eng Mater Technol*. 2020;142(4).

23. Woan K, Pyrgiotakis G, Sigmund W. Photocatalytic carbon-nanotube–TiO_2 composites. *Adv Mater*. 2009;21:2233–2239.

24. Wang WD, Serp P, Kalck P, et al. Visible light photodegradation of phenol on MWNT-TiO_2 composite catalysts prepared by a modified sol–gel method. *J Mol Catal A Chem*. 2005;235:194–199.

25. Serp P, Corrias M, Kalck P. Carbon nanotubes and nanofibers in catalysis. *Appl Catal A*. 2003;253:337–358.

26. Trocino S, Donato A, Latino M, et al. Pt-TiO_2/MWCNTs hybrid composites for monitoring low hydrogen concentrations in air. *Sensors*. 2012;12:12361-12373.

27. Tayel A, Ramadan AR, El Seoud OA. Titanium dioxide/graphene and titanium dioxide/graphene oxide nanocomposites: synthesis, characterization and photocatalytic applications for water decontamination. *Catalysts*. 2018;8(11):491.

28. Cullity BD. Elements of x-ray diffraction. London: Addison-Wesley Publishing Company Inc., 1978.

29. Ghadiry M, Gholami M, Lai CK, et al. Ultra-sensitive humidity sensor based on optical properties of graphene oxide and nano-anatase TiO_2. *PLoS ONE*. 2016;11:1–14.

30. Wang S, Cheng X. Solar photocatalytic degradation of typical indoor air pollutants using TiO_2 thin film codoped with iron(III) and nitrogen. *J Spectro*. 2015;2015.

31. Atchudan R, Pandurangan A, Joo J. Effects of nanofillers on the thermo-mechanical properties and chemical resistivity of epoxy nanocomposites. *J Nanosci Nanotechnol*. 2015;15:4255–4267.

32. Manna K, Srivastava SK. Contrasting role of defect-induced carbon nanotubes in electromagnetic interference shielding. *J Phys Chem C*. 2018;122:19913–19920.

33. Delekar SD, Dhodamani AG, More KV, et al. Structural and optical properties of nanocrystalline TiO_2 with multiwalled carbon nanotubes and its photovoltaic studies using Ru(II) sensitizers. *ACS Omega*. 2018;3:2743–2756.

34. Kamil AM, Hussein FH, Halbus AF, et al. Preparation, characterization, and photocatalytic applications of MWCNTs/TiO_2 composite. *Int J Photoenergy*. 2014;2014.

35. Ye S, Oh WC. Novel synthesis and characterization of Pt-graphene/TiO_2 composite designed for high photonic effect and photocatalytic activity under visible light. *J Korean Ceram Soc*. 2017;54:28–32.

36. Montero-Ocampo C, Vargas Garcia JR, Arce Estrada E. Comparison of TiO_2 and TiO_2-CNT as cathode catalyst supports for ORR. *Int J Electrochem Sci*. 2013;8:12780–12800.

37. Paunović P, Popovski O, Dimitrov AT, et al. Study of structural and electrochemical characteristics of Co-based hypo-hyper d-electrocatalysts for hydrogen evolution. *Electrochim Acta*. 2007;52:4640–4648.

38. Paunović P, Popovski O, Fidančevska E, et al. Co-Magneli phases electrocatalysts for hydrogen/oxygen evolution. *Int J Hydrogen Energy*. 2010; 35:10073–10080.

39. Paunović P, Popovski O, Stoevska Gogovska D, et al. Electrocatalytic activity of hypo-hyper d-electrocatalysts (Me/TiO_2/MWCNTs) based on Co-Ru in alkaline hydrogen electrolyzer. *Maced J Chem Chem Eng*. 2011;30:55–65.

40. Oshaka T, Izumi F, Y Fujiki. Raman spectrum of anatase TiO_2. *J Raman Spectrosc*. 1979;7:321–324.

41. Choi HC, Jung YM, Kim SB. Size effects in the Raman spectra of TiO_2 nanoparticles. *Vib Spectrosc*. 2005;37:33–38.

42. Parker JC, Siegel RW. Calibration of the Raman spectrum to the oxygen stoichiometry of nanophase TiO_2. *Appl Phys Lett*. 1990;57:943–945.

43. Bersani D, Lottici PP, Lopez T, et al. A Raman scattering study of $PbTiO_3$ and TiO_2 obtained by sol-gel,*J Sol-Gel Sci Technol*. 1998;13:849–853.

44. Mathpal MC, Tripathi AK, Singh MK, et al. Effect of annealing temperature on Raman spectra of TiO_2 nanoparticles. *Chem Phys Lett*. 2013;555:182–186.

45. Xu CY, Zhang PX, Yan L. Blue shift of Raman peak from coated TiO_2 nanoparticles. *J Raman Spectrosc*. 2001;32:862–865.

46. Gui MM, Chai SP, Xu BQ, et al. Visible-light-driven MWCNT@TiO2 core–shell nanocomposites and the roles of MWCNTs on the surface chemistry, optical properties and reactivity in CO_2 photoreduction. *RSC Advances*. 2014;4:24007–24013.

47. Saha A, Moya A, Kahnt A, et al. Interfacial charge transfer in functionalized multi-walled carbon nanotube@TiO_2 nanofibres. *Nanoscale*. 2017;9:7911–7921.

48. Dresselhaus MS, Dresselhaus G, Saito R, et al. Raman spectroscopy of carbon nanotubes. *Phys Rep*. 2005;409:47–99.

49. Lehman JH, Terrones M, Mansfield E, et al. Evaluating the characteristics of multiwall carbon nanotubes. *Carbon*. 2011;49:2581–2602.

50. Réti B, Mogyorósi K, Dombi A, et al. Substrate dependent photocatalytic performance of TiO_2/MWCNT photocatalysts. *Appl Catal A*. 2014;469:153–158.

51. Yurum A, Karakas G. Synthesis of Na-, Fe-, and Co-promoted TiO_2/multiwalled carbon nanotube composites and their use as a photocatalyst. *Turk J Chem*. 2017;41:440–454.

52. Zhang XX, Deng CF, Xu R, et al. Oxidation resistance of multi-walled carbon nanotubes purified with sulfuric and nitric acids. *J Mater Sci*. 2007; 42:8377–8380.

Citation: Paunović P, Grozdanov A, Makreski P, et al. Structural changes of TiO_2 as a result of CNTs incorporation. *Material Sci & Eng*. 2022;6(2):31–39.
DOI: 10.15406/mseij.2022.06.00177

53. Eder D, Windle AH. Morphology control of CNT-TiO2 hybrid materials and rutile nanotubes. *J Mater Chem*. 2008;18:2036–2043.

54. Zarezade M, Ghasemi S, Gholami MR. The effect of multiwalled carbon nanotubes and activated carbon on the morphology and photocatalytic activity of TiO2/C hybrid materials. *Catal Sci Technol*. 2011;1:279–284.

Citation: Paunović P, Grozdanov A, Makreski P, et al. Structural changes of TiO_2 as a result of CNTs incorporation. *Material Sci & Eng*. 2022;6(2):31–39.
DOI: 10.15406/mseij.2022.06.00177